IEEE Access
Multidisciplinary ⋮ Rapid Review ⋮ Open Access Journal

Received 23 January 2024, accepted 15 February 2024, date of publication 26 February 2024, date of current version 14 March 2024.

Digital Object Identifier 10.1109/ACCESS.2024.3370677

RESEARCH ARTICLE

A Reduced-Order Robust Wide-Area Damping Control for Wind-PV-Thermal-Bundled Power System Considering Operational Uncertainties and Communication Resilience

ZHEN WANG, (Member, IEEE), REHAN SADIQ, AND DEQIANG GAN, (Senior Member, IEEE)
College of Electrical Engineering, Zhejiang University, Hangzhou 310058, China
Corresponding author: Zhen Wang (z.wang@zju.edu.cn)

This work was supported by the National Natural Science Foundation of China under Grant 52077196.

ABSTRACT The wind-photovoltaic-thermal-bundled power system (WPTBS) comes with a wide range of potential grid applications and provides an efficient way to export bulk amount of power under high intermittency of wind and photovoltaic (PV) resources. This increasing penetration alongside distant power transmission, however, may cause detrimental impacts on low-frequency oscillations (LFOs), eventually threatening the stability of WPTBS. In this prospect, installing a wide-area damping controller (WADC) is proven to be efficient in suppressing LFOs but the uncertainty related to varying operating points, the time delay involved in transmitting a wide-area signal, and the possibility of remote signal disconnection may compromise the damping capability of a WADC. Following that, the proposed study presents a reduced-order robust wide-area damping controller (RWDC), injected into the wind turbine system, to stabilize the LFOs in the WPTBS while accounting for operational uncertainties, time delays, and communication failure. At first, the uncertainties are characterized in the form of polytope vertices, where each vertex represents a linearized model corresponding to a distinct operating condition. A two-stage linear matrix inequality (LMI) approach is then adopted to determine the design parameters of reduced-order RWDC, which simultaneously stabilizes the entire uncertain model by minimizing the H_∞ norm and ensures closed-loop stability via parameter-dependent Lyapunov functions. Finally, using small-signal analysis and extensive simulation results, the effectiveness of the controller is confirmed under different operating scenarios, including critical and unstable oscillation conditions, followed by a comparison with existing methods.

INDEX TERMS Renewable integration, wide-area oscillation damping, linear matrix inequalities (LMIs), reduced-order H_∞ control, power system uncertainties.

NOMENCLATURE

WPTBS	Wind-photovoltaic-thermal-bundled power system.
PV	Photovoltaic.
LFOs	Low-frequency oscillations.
WADC	Wide-area damping controller.
RWDC	Robust wide-area damping controller.
LMI	Linear matrix inequality.
PMUs	Phasor measurement units.
IAMs	Inter-area modes.
FACTS	Flexible AC transmission systems.
PSO	Particle swarm optimization.
PDLF	Parameter-dependent Lyapunov function.
SG	Synchronous generator.
DFIG	Doubly-fed induction generator.
GSC	Grid side converter.
MPPT	Maximum power-point tracking.
VSI	Voltage source inverter.
LTI	Linear time-invariant.

The associate editor coordinating the review of this manuscript and approving it for publication was Yonghao Gui.

OFC Output feedback controller.
GMO Geometric measure of observability.
SMA Selective modal analysis.

I. INTRODUCTION

In the past decade, owing to increased electricity demand and environmental concerns related to fossil fuel-based resources, enormous efforts have been devoted to integrating renewable energy generation into the power grid, primarily to deliver clean energy at a low cost [1]. Wind and photovoltaic (PV) energy systems dominate among the rapidly growing renewable resources in the world. Particularly, China is leading in terms of installed wind and PV resource capacities, where large-scale wind and PV farms in some regions are coupled together with conventional thermal generators to form a wind-PV-thermal-bundled power system (WPTBS) for transmitting the bulk amount of power via long-distant AC/DC transmission lines [2], [3]. The WPTBS offers additional generation control support and reduces the impact of intermittent behavior in wind and PV systems to provide smooth power transmission, thereby ensuring stability and improving the reliability of the modern power grid by maximizing the availability of renewable resources [2], [4].

To cope with the increasing energy demand, significant penetration of these renewables could, however, result in network congestion, eventually disrupting the small-signal stability of the power network [1]. Moreover, uncertainty in the power outputs of these renewables, together with the fluctuating load and change in thermal generation demands can affect the network power flows. Subsequently, in such situations, low-frequency oscillations (LFOs) will be of great concern since poor damping of these modes could threaten the stability of the large interconnected system [5], [6]. Hence, investigating the small-signal stability of WPTBS under uncertain operating conditions and suppressing LFOs is crucial to sustaining the satisfactory dynamic performance of the system undergoing disturbance [7]. Installing a wide-area damping controller (WADC) in this respect provides a frequently adopted solution to maintain the system's sufficient damping performance [8]. On the other hand, synthesizing the WADC mainly involves acquiring remote feedback signals via phasor measurement units (PMUs), owing to their high observability for the LFOs, especially inter-area modes (IAMs). Also, PMUs utilize a communication network for transmitting wide-area signals to the controller's location; hence, the possibility of channel latency and communication failure always exists, which would severely deteriorate the damping performance of the WADC or even cause closed-loop instability under loss of feedback signal [9].

A. LITERATURE REVIEW

To address such issues, various studies have been carried out in the recent decade to design WADCs and such investigations are still under constant development. A machine learning-based robust coordinated WADC was recently proposed in [10] by establishing an uncertainty model of the power system. The design of a WADC for flexible AC transmission systems (FACTS) was presented in [11] to determine the gain by calculating the delay margin using linear matrix inequality (LMI) criteria. Nevertheless, because of the risks involved in the failure of communication channels, employing one wide-area signal cannot assure system reliability. Accordingly, the WADC based on a robust control approach [12] and heuristic dynamic programming [13] was constructed using multiple feedback signals to tolerate communication failures. To provide robustness under operating point uncertainties, time delays, and communication failures, a hybrid particle swarm optimization (PSO) [8] and the LMI framework with pole-placement constraint [9] were adopted. But, the previous works [8], [9], [11], [12], [13] have not addressed the dynamics associated with the wind or PV systems. Also, the hybrid optimization procedure presented in [8] involves integrating the mutation operator of a genetic algorithm into the PSO; though it provides improved performance, it requires tuning an additional parameter during each iteration, thereby increasing the overall complexity of the algorithm. Besides, defining the pole-placement constraint in the LMI approach [9] to accomplish the required damping of the critical modes may degrade other modes with higher damping than the specified pole-placement. Also, the methodology corresponds to the conservative perspective of guaranteeing quadratic stability by using a fixed Lyapunov function for the entire uncertain model. To stabilize renewable-integrated power systems, some researchers have applied metaheuristic algorithms to determine damping controller parameters for FACTS [2], [14], [15]. Nevertheless, uncertainties and communication-related issues have not been taken into account while designing the controller. A multi-objective LMI-based approach is presented in [1] for the stability enhancement of offshore/onshore wind farm-based power networks by addressing uncertainties via a polytopic model. However, the work does not account for time delays and feedback signal failures.

In recent years, most studies [4], [7], [16], [17], [18], [19], [20], [21], [22] have focused on exploiting the damping capability of wind farms or PV systems owing to the high cost involved in installing FACTS, the displacement of conventional generators with renewable resources, and the need to provide ancillary services via converter-based resources demanded by transmission operators. The damping contribution from large-scale wind/PV systems can be achieved by modulating active power [21], reactive power/voltage [7], [16], [17], or dual-control loops [4], [19], [20]. In this context, some researchers aimed primarily at highlighting the effectiveness of active/reactive power coordination or presenting a novel active power modulation strategy for utility-scale wind and/or PV systems [4], [20], [21]. Nevertheless, system uncertainties and communication-related issues are also crucial aspects to be considered. The performance of an adaptive

WADC controller is validated in [17] for the wind power system. The uncertainties in the design process are accommodated by adopting multiple models based on a Bayesian framework, whereas the time delays are compensated using the Padé approximation. The delay-dependent LMI techniques can also be adopted to account for time delays and communication failures in the design of WADC for wind or PV systems [16], [19]. However, the work presented in [16] considered a combination of local and remote signals to counteract the communication failure, which may not guarantee the minimum damping level in the event of wide-area signal loss. Furthermore, regarding wind/PV uncertainties, the LMI-based gain scheduling control [23] and a decentralized coordinated control [24] were also presented without considering the communication failure.

B. MOTIVATIONS AND CONTRIBUTIONS

Based on the aforementioned literature, the following factors motivate the authors to conduct the proposed research: 1) With the evolving modern power grid, it has become essential to build a robust wide-area damping controller (RWDC) that accounts for the uncertainties and dynamics of wind and PV resources, followed by incorporating the time delays and wide-area signal failures. 2) to synthesize a reduced-order controller, which would be easier to implement in practice compared to the higher-order controllers [1], [24], and provides more degree of freedom in design parameters than the static gain controller [19] without measuring the system's states as required by the state feedback controller [10], [23]. 3) to adopt a less-conservative LMI framework [25], which guarantees robust stability for the complete uncertain model using parameter-dependent Lyapunov functions (PDLFs) instead of a common Lyapunov function [9], [23]. Following this, the main contributions of the proposed study are outlined below:

1) This article presents a RWDC for the WPTBS to mitigate LFOs by assuring robustness against uncertain operating conditions, time delays, and permanent loss of feedback signals.
2) A polytopic model based on a typical set of operating points is constructed to accommodate the uncertainties in the load demands and power outputs of wind/PV systems and conventional generators, followed by incorporating the time delays and communication failures in the design of RWDC.
3) The proposed work adopts a two-stage parameter-dependent LMI framework to design a reduced-order H_∞ dynamic output feedback controller that simultaneously ensures the asymptotic stability of the entire polytopic model based on Lyapunov functions of assigned degrees. The robustness of the controller under multiple operating conditions involving unstable mode, the worst-case scenario, and comparison with existing approaches validate the dominance of the proposed approach.

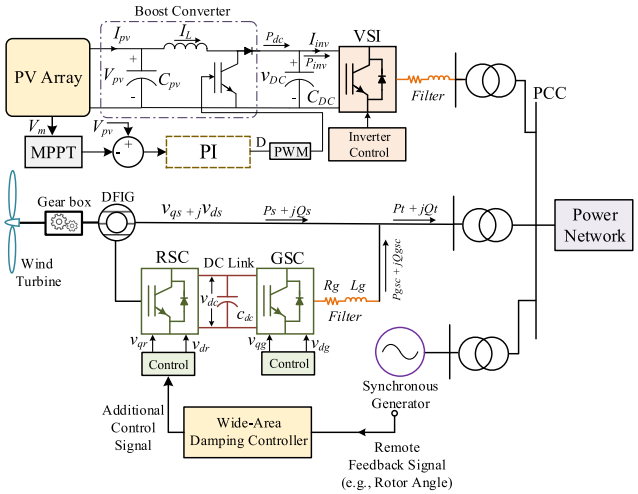

FIGURE 1. Configuration of the wind-PV-thermal-bundled power system.

II. MODELING AND CONTROL ARCHITECTURE

The configuration of the WPTBS is shown in Fig 1, where the large-scale thermal generator, aggregated wind farm, and PV system are connected to the power network through step-up transformers [2], [3]. In this work, the dynamics of the thermal generator are characterized by a conventional synchronous generator (SG). The sub-transient sixth-order dynamic model constitutes the representation of each SG in the power network, followed by the installation of static exciters (*IEEE ST1A*) on all generators [26]. Besides, the wind farm is modeled as a doubly-fed induction generator (DFIG). The details about the DFIG and a PV system are presented below.

A. DFIG MODEL

The basic construction of the DFIG contains the dynamic model of the turbine and drive train, induction generator, rotor side converter (RSC), and grid side converter (GSC) along with the DC-link. The electrical dynamics of the generator, represented in the d-q (direct-quadrature) axis reference frame, are given as follows [27]:

$$\begin{aligned}
\frac{di_{qs}}{dt} &= \frac{\omega_{el}}{L'_s}(-R_1 i_{qs} + \omega_s L'_s i_{ds} + \frac{\omega_r}{\omega_s} e'_{qs} - \frac{1}{T_r \omega_s} e'_{ds} \\
&\quad - v_{qs} + K_{mrr} v_{qr}) \\
\frac{di_{ds}}{dt} &= \frac{\omega_{el}}{L'_s}(-R_1 i_{ds} - \omega_s L'_s i_{qs} + \frac{\omega_r}{\omega_s} e'_{ds} + \frac{1}{T_r \omega_s} e'_{qs} \\
&\quad - v_{ds} + K_{mrr} v_{dr}) \\
\frac{de'_{qs}}{dt} &= \omega_{el}\omega_s(R_2 i_{ds} - \frac{e'_{qs}}{T_r \omega_s} + \left(1 - \frac{\omega_r}{\omega_s}\right) e'_{ds} - K_{mrr} v_{dr}) \\
\frac{de'_{ds}}{dt} &= \omega_{el}\omega_s(-R_2 i_{qs} - \frac{e'_{ds}}{T_r \omega_s} - \left(1 - \frac{\omega_r}{\omega_s}\right) e'_{qs} + K_{mrr} v_{qr})
\end{aligned} \tag{1}$$

where $R_1 = R_s + R_2$, $R_2 = K_{mrr}^2 R_r$, $K_{mrr} = L_m / L_r$, $T_r = L_r / R_r$, $L'_s = L_s - (L_m{}^2 / L_r)$, $e'_{qs} = K_{mrr} \omega_s \psi_{dr}$,

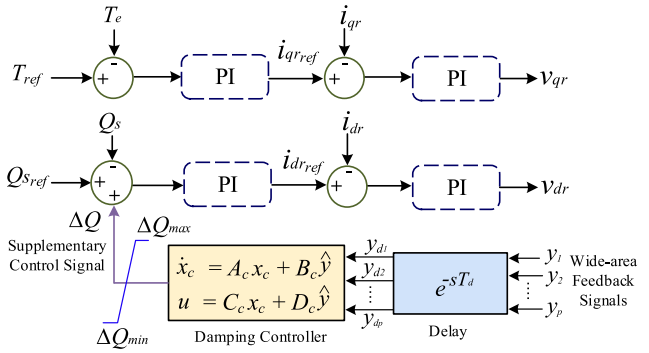

FIGURE 2. Control structure of the RSC.

$e'_{ds} = -K_{mrr}\omega_s\psi_{qr}$. The variables R_s and L_s are the stator resistance and inductance; R_r and L_r denote rotor resistance and inductance; L_m is the mutual inductance between the stator and rotor; e'_{qs} and e'_{ds} stand for transient voltages; and i_{ds}, i_{qs}, ψ_{dr}, ψ_{qr}, v_{dr} and v_{qr} are the d-axis and q-axis components of the stator current, rotor flux, and rotor voltage, respectively. The converters' control approach comprises a decoupled vector control scheme, which allows for the independent control of active and reactive power control via cascaded control loops. For the RSC, the q- and d-axis control loops, respectively, establish the torque/active power and reactive power control, as depicted in Fig 2. The rotor current references $i_{qr_{ref}}$ and $i_{dr_{ref}}$ generated by the outer q- and d-axis control loops are used to produce rotor voltage references via fast inner-current control loops. In addition, the supplementary control signal ΔQ supplied by the RWDC is injected at the outer d-axis loop to modulate the reactive power for damping purposes. Further details regarding the dynamics and control of the converters can be found in [15], [16], and [27].

B. PV SYSTEM MODEL

One of the widely used structures of a two-stage PV plant comprises PV arrays, a boost converter with maximum power-point tracking (MPPT) control, a DC-link capacitor, and a voltage source inverter (VSI) as shown in Fig 1 [19]. The DC/DC converter not only captures the maximum power from the PV panels using the MPPT algorithm but also boosts the voltage to an appropriate level for the DC link. On the other hand, the VSI delivers power to the grid by maintaining constant DC-link voltage and power balance between the DC and AC sides [28]. The proposed work utilizes a 100 MW aggregated PV plant constructed by connecting several parallel N_p and series N_s strings. The parameters of the PV array are referred to [28]. The model of a PV array is represented by the practical engineering model based on a single diode, described by the following current-voltage (I_{pv} - V_{pv}) relationship [28]:

$$I_{pv} = N_p I_{sc}\left[1 - C_1\left(e^{V_{pv}/(C_2 N_s V_{oc})} - 1\right)\right]$$
$$C_1 = \left(1 - I_m/I_{sc}\right)e^{-V_m/(C_2 V_{oc})}$$
$$C_2 = (V_m/V_{oc} - 1)/ln\left(1 - I_m/I_{sc}\right) \quad (2)$$

where V_{oc}, I_{sc}, V_m, and I_m, respectively, denote the open-circuit voltage, short-circuit current, voltage, and current at the maximum power point, specified by the manufacturer; and C_1 and C_2 are constants. The dynamics of the boost converter, based on the average switching model, are represented by (3) as follows:

$$\dot{V}_{pv} = \frac{1}{C_{pv}}(I_{pv} - I_L)$$
$$\dot{I}_L = \frac{1}{L_b}\left[V_{pv} - (1 - D)v_{dc}\right] \quad (3)$$

where v_{dc} is the DC-link voltage; L_b and I_L are the inductance and inductor current, respectively; and C_{pv} and D are the capacitance and duty cycle of the boost converter, respectively. The decoupled dq-axis control of the VSI can be accomplished using the outer/inner control loops, similar to the DFIG, as stated previously [4], [28].

Finally, the complete linear time-invariant (LTI) model of the WPTBS, containing system states ($x \in R^n$), system input ($u \in R^r$) and measured output ($y \in R^p$), is denoted as follows:

$$\dot{x} = Ax + Bu$$
$$y = Cx$$
$$x = \left[x_{SG}^T \quad x_{DFIG}^T \quad x_{PV}^T\right]^T, \quad u = [\Delta Q]^T \quad (4)$$

C. POLYTOPIC UNCERTAINTY REPRESENTATION

The uncertainty in the operating point of the WPTBS disturbs the damping of LFOs owing to irregular wind/PV penetration, different power levels of SGs, and fluctuating load demands. For that purpose, taking uncertainties into account during the design stage of the controller is an efficient way to ensure acceptable damping performance under a wide operating region. Accordingly, based on system (4), the uncertain model of the WPTBS is described by:

$$\dot{x} = A(\alpha)x + B(\alpha)u$$
$$y = C(\alpha)x \quad (5)$$

The uncertain matrices $A(\alpha)$, $B(\alpha)$, and $C(\alpha)$, which are time-invariant, correspond to the polytope domain $\mathcal{P}$ such that $(A, B, C)(\alpha) \in \mathcal{P}$ and are expressed as follows:

$$\begin{cases} \mathcal{P} = \mathbb{C}\{\mathcal{P}_1, \mathcal{P}_2, \ldots \mathcal{P}_N\} \\ = \left\{\sum_{j=1}^{N} \alpha_j \mathcal{P}_j : \sum_{j=1}^{N} \alpha_j = 1, \alpha_j \geq 0\right\} \end{cases} \quad (6)$$

with

$$\mathcal{P}_j = [A_j, B_j, C_j], \; j = 1, 2 \ldots N$$

where $\mathbb{C}$ denotes the convex hull; N is the total number of polytope vertices $\mathcal{P}_j$; and α_j indicates polytopic coordinate. The convex combinations of these vertices $\{\mathcal{P}_1, \mathcal{P}_2, \ldots \mathcal{P}_N\}$ formulate a polytope $\mathcal{P}$, where each vertex indicates an LTI model corresponding to a typical operating point of the WPTBS. Due to the convex property of the polytope, once the

control law is established by satisfying LMI conditions for each vertex, the synthesized controller can guarantee robust performance for all other vertices lying within the same polytope.

D. WIDE-AREA DAMPING CONTROLLER

The WADC mainly employs PMUs to obtain remote feedback signals, which are then transmitted to the controller's location via communication channels. Subsequently, the unavoidable delays associated with the wide-area signal transmission should be approximated during the design process of the controller to maintain its acceptable damping level. On the other hand, wide-area feedback signals, though more effective than local signals, are susceptible to cyberattacks, causing the failure of communication channels. Thus, in the absence of a feedback signal, the controller will be unable to perform damping control actions, subsequently deteriorating the reliability of the WPTBS. Hence, a robust damping controller must operate with more than one wide-area signal to provide resiliency in the event that one of the feedback signals fails.

1) TIME DELAY APPROXIMATION

The time delays e^{-sT_d} are modeled using the Padé approximation with the below-mentioned second-order transfer function [8], [17].

$$G_d(s) = \frac{6 - 2T_d s}{6 + 4T_d s + (sT_d)^2} \tag{7}$$

where T_d denotes the time delay value. The model $G_d(s)$ in state-space form is given by:

$$\begin{aligned} \dot{x}_d &= A_d x_d + B_d u_d \\ y_d &= C_d x_d \end{aligned} \tag{8}$$

with

$$A_d = \begin{bmatrix} 0 & -6/T_d^2 \\ 1 & -4/T_d \end{bmatrix}, \quad B_d = \begin{bmatrix} 6/T_d^2 \\ -2/T_d \end{bmatrix}, \quad C_d = \begin{bmatrix} 0 \\ 1 \end{bmatrix}^T$$

where x_d, u_d, and y_d indicate vectors of delay states, input, and output, respectively. By combining (5) and (8), the following represents the uncertain dynamic model of the WPTBS including time delays:

$$\begin{aligned} \dot{\hat{x}} &= \hat{A}_j \hat{x} + \hat{B}_j u \\ \hat{y} &= \hat{C}_j \hat{x} \end{aligned} \tag{9}$$

where

$$\hat{x} = [\, x \quad x_d \,]^T,$$
$$\hat{A}_j = \begin{bmatrix} A_j & 0 \\ B_d C_j & A_d \end{bmatrix}, \ \hat{B}_j = \begin{bmatrix} B_j \\ B_d \end{bmatrix},$$
$$\hat{C}_j = \begin{bmatrix} C_j \\ C_d \end{bmatrix}^T$$

and $\hat{x} \in \mathcal{R}^{n+n_d}$, n_d refers to the order of approximated delay model, and $\hat{y} = \begin{bmatrix} y_{d1} & y_{d2} & \dots & y_{dp} \end{bmatrix}^T$ denotes a vector of delayed wide-area measured outputs.

2) LOSS OF WIDE-AREA FEEDBACK SIGNALS

The permanent communication failure indicates that for p system outputs (*i.e.*, $k = 1, 2 \dots p$), the kth row of the output matrix $\hat{C}_j \in \mathcal{R}^{p \times n}$ relevant to the lost wide-area signal becomes zero [8]. If the matrix $\hat{C}_j$ is given by:

$$\hat{C}_j = \begin{bmatrix} \hat{c}_{1j}^T & \hat{c}_{2j}^T & \cdots & \hat{c}_{pj}^T \end{bmatrix}^T \tag{10}$$

then $\hat{c}_{kj} \in R^{1 \times n}$ denotes the kth output. To represent loss of wide-area signal, the matrix $\hat{C}_j$ of (9) is updated as follows [29]:

$$\begin{aligned} \hat{C}_j^i &= \begin{bmatrix} \hat{c}_{1j}^{i\,T} & \hat{c}_{2j}^{i\,T} & \cdots & \hat{c}_{pj}^{i\,T} \end{bmatrix}^T \\ \hat{c}_{kj}^i &= \begin{cases} 0 & \text{if } i = k \\ \hat{c}_{kj} & \text{if } i \neq k \end{cases} \end{aligned} \tag{11}$$

where $i = 0, 1, \dots, p$ and $k = 1, 2, \dots, p$. Based on (11), the proposed approach can select multiple feedback signals and various communication failures simultaneously. For simplicity, in this work, two wide-area signals are considered, with the loss of one signal at a time, which are expressed as follows:

$$\hat{C}_j^i = \begin{cases} \hat{C}_j^0 = \begin{bmatrix} \hat{c}_{1j}^T & \hat{c}_{2j}^T \end{bmatrix}^T = \hat{C}_j \\ \hat{C}_j^1 = \begin{bmatrix} 0 & \hat{c}_{2j}^T \end{bmatrix}^T \\ \hat{C}_j^2 = \begin{bmatrix} \hat{c}_{1j}^T & 0 \end{bmatrix}^T \end{cases} \tag{12}$$

where $i = 0$, $i = 1$, and $i = 2$, respectively, stand for no communication failure, loss of signal y_{d1}, and y_{d2} With the new $\hat{C}_j^i$ matrix (12), the system (9) is modified as given below:

$$\begin{aligned} \dot{\hat{x}} &= \hat{A}_j^i \hat{x} + \hat{B}_j u \\ \hat{y} &= \hat{C}_j^i \hat{x} \end{aligned} \tag{13}$$

Considering model (13) of WPTBS, the present study seeks a RWDC to ensure robustness against operating point uncertainty, time delay, and permanent loss of remote feedback signal.

3) CONTROL STRUCTURE

The proposed study intends to design a robust reduced-order dynamic output feedback controller (OFC) K_c, as depicted in Fig 2, which can be expressed by the dynamical system (14) or using matrix form (15) [25].

$$\begin{aligned} \dot{x}_c &= A_c x_c + B_c \hat{y} \\ u &= C_c x_c + D_c \hat{y} \end{aligned} \tag{14}$$

$$K_c = \begin{bmatrix} A_c & B_c \\ C_c & D_c \end{bmatrix} \tag{15}$$

where x_c indicates the controller's state vector of the order $n_c \geq 0$. Next, the LMI approach will be presented to determine the parameters of the controller (15).

III. PARAMETER DEPENDENT LYAPUNOV FUNCTION-BASED TWO-STAGE LMI APPROACH

A. APPROACH PRINCIPLE

Following the traditional robust control approach, the continuous-time augmented state-space representation of the uncertain model (13) is presented as follows [25]:

$$\begin{aligned}\dot{\hat{x}} &= \hat{A}_j^i\hat{x} + \hat{B}_{1j}w + \hat{B}_{2j}u\\ z &= \hat{C}_{1j}^i\hat{x} + \hat{D}_{1j}w + \hat{D}_{2j}u\\ \hat{y} &= \hat{C}_{2j}^i\hat{x} + \hat{D}_{yj}w\end{aligned} \tag{16}$$

where w and z refer to external disturbance and controlled output, respectively. The design problem of reduced-order K_c can be converted into determining a static output feedback gain matrix $K_c \in R^{(r+n_c)\times(n_c+p)}$. However, formulating a problem using this approach may cause A_c matrix of (15) to become block diagonal with $B_c = C_c = 0$, thus yielding only a static gain controller when $n_c > 0$ [30]. Therefore, to avoid such numerical issues, the following similarity transformation is used [30]:

$$\begin{bmatrix}\bar{\hat{x}}\\ \bar{x}_c\end{bmatrix} = \begin{bmatrix}I_n & 0\\ T & I_{n_c}\end{bmatrix}\begin{bmatrix}\hat{x}\\ x_c\end{bmatrix}, T = \begin{bmatrix}I_{n_c} & 0_{n_c\times(n-n_c)}\end{bmatrix} \tag{17}$$

Based on the system (16) and transformation (17), the augmented system including controller states is given below:

$$\begin{aligned}\dot{\eta} &= \tilde{A}_j^i\eta + \tilde{B}_{1j}w + \tilde{B}_{2j}\\ z &= \tilde{C}_{1j}^i\eta + \tilde{D}_{1j}w + \tilde{D}_{2j}u\\ \hat{y} &= \tilde{C}_{2j}^i\eta + \tilde{D}_{yj}w\end{aligned} \tag{18}$$

where

$$\eta = \begin{bmatrix}\bar{\hat{x}}\\ \bar{x}_c\end{bmatrix},\ \tilde{A}_j^i = \begin{bmatrix}\hat{A}_j^i & 0\\ T\hat{A}_j^i & 0_{n_c}\end{bmatrix},\ \tilde{B}_{1j} = \begin{bmatrix}\hat{B}_{1j}\\ T\hat{B}_{1j}\end{bmatrix}$$
$$\tilde{B}_{2j} = \begin{bmatrix}0 & \hat{B}_{2j}\\ -I_{n_c} & T\hat{B}_{2j}\end{bmatrix},\ \tilde{C}_{1j}^i = \begin{bmatrix}\hat{C}_{1j}^i & 0\end{bmatrix},$$
$$\tilde{C}_{2j}^i = \begin{bmatrix}I_{n_c}T & -I_{n_c}\\ \hat{C}_{2j}^i & 0\end{bmatrix}$$
$$\tilde{D}_{1j} = \begin{bmatrix}\hat{D}_{1j}\end{bmatrix},\ \tilde{D}_{2j} = \begin{bmatrix}0 & \hat{D}_{2j}\end{bmatrix},\ \tilde{D}_{yj} = \begin{bmatrix}\hat{D}_{yj}\\ 0\end{bmatrix}$$

Correspondingly, the closed-loop system matrices become:

$$\begin{aligned}\tilde{A}_{cl,j} &= \tilde{A}_j^i + \tilde{B}_{2j}K_c\tilde{C}_{2j}^i\\ \tilde{B}_{cl,j} &= \tilde{B}_{1j} + \tilde{B}_{2j}K_c\tilde{D}_{yj}\\ \tilde{C}_{cl,j} &= \tilde{C}_{1j}^i + \tilde{D}_{2j}K_c\tilde{C}_{2j}^i\\ \tilde{D}_{cl,j} &= \tilde{D}_{1j} + \tilde{D}_{2j}K_c\tilde{D}_{yj}\end{aligned} \tag{19}$$

If the H_∞ norm of the closed-loop transfer function $M_{zw}(s)$ from w to z is denoted by $\|M_{zw}(s)\|_\infty$ and there exists a scalar $\gamma > 0$, then the control objective implies designing a reduced-order robust dynamic OFC, which satisfies the following H_∞ performance criteria:

$$\|M_{zw}(s)\|_\infty < \gamma \tag{20}$$

with

$$M_{zw}(s) = \tilde{C}_{cl,j}\left(sI - \tilde{A}_{cl,j}\right)^{-1}\tilde{B}_{cl,j} + \tilde{D}_{cl,j} \tag{21}$$

The LMI approach adopted in the proposed work involves two stages [25]. During the first step, a parameter-dependent state-feedback gain K_j^{sf} is computed, which is then used in the second stage to synthesize a common dynamic OFC K_c of pre-defined order for the entire polytope. Both stages of the LMI approach exploit the PDLFs of arbitrary degrees. This implies that the closed-loop stability is guaranteed with a PDLF $U(x) = x^{\mathrm{T}}P_jx$ when a positive definite matrix $P_j = P_j^{\mathrm{T}} > 0$ is obtained by satisfying the LMI constraints [31]. Based on the conclusion drawn in [25], the proposed approach for H_∞ stabilization can be stated by the two-stage parameter-dependent LMI conditions below.

Stage 1: For a known scalar $\mu > 0$, if there exist parameter-dependent matrices $P_j = P_j^T > 0$, Z_j, and a matrix G then the following LMI conditions must be satisfied [25]:

$$\begin{bmatrix}He\left(\tilde{A}_j^iG + \tilde{B}_{2j}Z_j\right) & *\\ P_j - G_j + \mu\left(\tilde{A}_j^iG_j + \tilde{B}_{2j}Z_j\right)^T & -\mu\left(He\left(G\right)\right)\end{bmatrix} < 0$$
$$P_j > \varepsilon I \tag{22}$$

where $He(A) = A + A^T$; $\varepsilon = 1$, and $*$ denotes the respective symmetric terms in block matrices. Afterward, the parameter-dependent state-feedback controller K_j^{sf} stabilizing the system (18) is obtained as follows:

$$K_j^{sf} = Z_j(G)^{-1} \tag{23}$$

The parameter μ provides an additional degree of freedom and allows to construct distinct K_j^{sf}. By performing the search on μ with 13 values evenly spaced on a logarithm scale in the range $[10^{-6}, 10^6]$, its optimal value can be selected [25]. This can be accomplished by executing the MATLAB command logspace(−6, 6, 13).

Stage 2: For a scalar $\gamma > 0$, if there exist matrices $Q_j = Q_j^T > 0$, R, L, H_j, V_j, and F_j with known K_j^{sf} such that the LMI conditions given (24) is valid [25].

$$\begin{bmatrix}\varphi_{11} & \varphi_{12} & \varphi_{13} & \varphi_{14} & \varphi_{15}\\ * & -He\left(V_j\right) & V_j\tilde{B}_{1j} & 0 & V_j\tilde{B}_{2j}\\ * & * & -\gamma^2I & \tilde{D}_{1j}^TH_j & \tilde{D}_{yj}^TL^T\\ * & * & * & I - He\left(H_j\right) & H_j^T\tilde{D}_{2j}\\ * & * & * & * & -He\left(R\right)\end{bmatrix} < 0$$
$$Q_j > 0 \tag{24}$$

Then, the robust dynamic OFC, with guaranteed H_∞ performance level γ, is determined by (25).

$$K_c = R^{-1}L \tag{25}$$

where

$$\varphi_{11} = He(F_j(\tilde{A}_j^i + \tilde{B}_{2j}K_j^{sf}))$$
$$\varphi_{12} = Q_j - F_j + (\tilde{A}_j^i + \tilde{B}_{2j}K_j^{sf})^TV_j^T$$

$$\varphi_{13} = F_j \tilde{B}_{1j}$$
$$\varphi_{14} = (\tilde{C}_{1j}^{i})^{T} H_j + (K_j^{sf})^{T} \tilde{D}_{2j}^{T} H_j$$
$$\varphi_{15} = F_j \tilde{B}_{2j} + (\tilde{C}_{2j}^{i})^{T} L^{T} - (K_j^{sf})^{T} R^{T}$$

In the above LMI conditions, the matrix variables H_j, V_j, and F_j have been considered as homogenous polynomials of fixed degree one. However, for the Lyapunov matrices P_j and Q_j in stage 1 and stage 2, along with the matrix Z_j of stage 1, different values of their polynomial degree can be selected and indicated by a set $g = \{ g_P \; g_Q \; g_Z \}$, respectively.

B. ALGORITHM TO SYNTHESIZE CONTROLLER

The algorithm for determining controller parameters using the proposed LMI scheme is outlined below:

Step 1 Initialization: Define N distinct operating points of the WPTBS to account for operational uncertainties and select wide-area feedback signals.

Step 2 Uncertain System Modeling: Establish an uncertain model (5) by constructing vertices of the polytope (6) with a given set of operating points.

Step 3 Model Reduction: Reduce the order of the model by using the selective modal analysis (SMA) method [10], [23].

Step 4 Communication Resilience Modeling: Expand the uncertain reduced-order model (5) to incorporate fixed-time delays and wide-area communication failure in accordance with (9) and (13), respectively.

Step 5 Solving Two-stage LMI Problem: Set $g = \{ g_P \; g_Q \; g_Z \}$, $n_c \geq 0$, and $\mu > 0$ and solve LMIs (22) and (24) in Stages 1 and 2, respectively, with the objective function of minimizing γ.

Step 6 Controller Parameter Determination: Obtain the parameters of the dynamic OFC K_c using (25).

Step 7 Stability Evaluation: Confirm close-loop stability for the entire set of vertices using (19). If the required damping level is obtained for each vertex, STOP; otherwise, change the values of μ, g, and n_c, and repeat Steps 5 to 7.

IV. SYSTEM STUDY AND CONTROLLER IMPLEMENTATION

The proposed methodology is validated on a modified two-area benchmark system [32], as depicted in Fig 3. The wind and PV systems, having 200 MW and 100 MW of capacity, respectively, are connected in Area 1 alongside G_2 at bus 6 to represent a WPTBS. Based on this network configuration, Area 2 heavily imports active power of 500 MW from Area 1 via 220 km tie-lines.

A. DEFINING OPERATING POINTS AND ANALYZING SMALL-SIGNAL STABILITY

To design a damping controller robust against a wide-operating region of the WPTBS, a set of N typical operating conditions must be considered to construct vertices $\{[A_1, B_1, C_1], [A_2, B_2, C_2], \ldots [A_N, B_N, C_N]\}$ of the polytopic uncertain model. Accordingly, the proposed work intends to design RWDC by considering following operating points, expressed as follows:

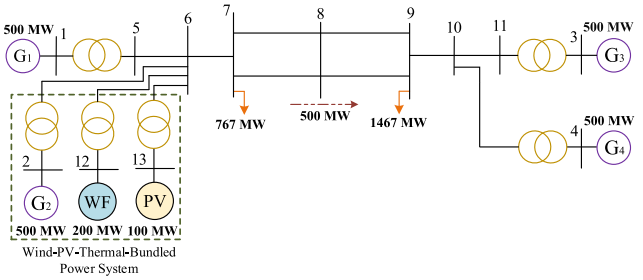

FIGURE 3. Modified benchmark system.

- p_1: The nominal or base case where Area 2 is receiving 500 MW power from Area 1, as depicted in Fig 3.
- p_2: Low penetration case during which the power outputs of wind, PV, and G_2 are reduced by 75%, 50%, and 10%, respectively, from their nominal values, decreasing load demand at buses 7 and 9 by 150 MW each, and exporting 400 MW of power from Area 1 to Area 2.
- p_3: High penetration case established by raising the power levels of G_1 and G_2 by 20% each, a 10% increase in the power output of G_3, adding 100 MW and 200 MW of load to buses 7 and 9, respectively, and delivering 600 MW of power through tie-lines.
- UOP: An unstable operating point (UOP) case formed by permanently tripping one of the tie-lines linking bus 8 and bus 9, a 20% increase in the power output of G_3, and a 300 MW increase in the load value at bus 9, relative to the base values.

The UOP, which is not one of the polytope vertices, will only be used to validate the controller's effectiveness under unstable oscillation. The small-signal analysis is then conducted to analyze the critical modes. The eigenvalue plot, shown in Fig 4, illustrates that local modes are adequately damped. However, the damping ratio (ζ) of the IAM remains below 5% for all operating conditions stated above and severely deteriorates with increased penetration of wind-PV-thermal resources, and can become unstable (as listed in TABLE 1), eventually jeopardizing the stability of the WPTBS. On account of this, the present study emphasizes designing a dynamic OFC by simultaneously stabilizing the complete set of vertices to provide robustness against uncertain operating points.

B. WIDE-AREA SIGNAL SELECTION

To ensure the optimal performance of the controller, the input feedback signal should be appropriately selected. For resiliency against permanent wide-area communication failure, two feedback signals are considered. These wide-area feedback signals are selected based on their geometric measure of observability (GMO) to the critical IAM [17]. By taking various candidate signals such as the rotor angles

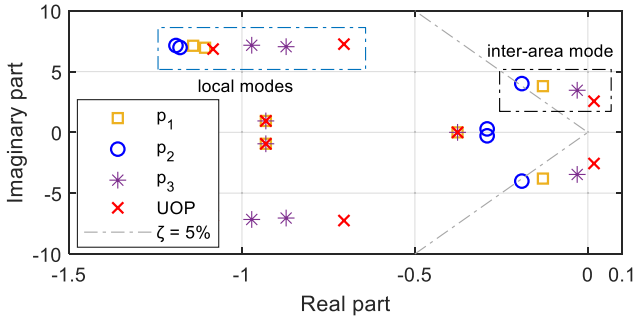

FIGURE 4. Eigenvalue plot for the open-loop system.

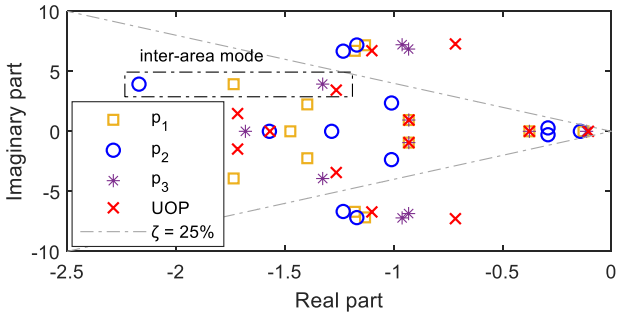

FIGURE 5. Eigenvalue plot for different operating points.

TABLE 1. Dominant inter-area mode for the WTBPS under different operating points.

Operating points	Eigenvalues	Damping ratios (%)	Frequency (Hz)
p_1	-0.1299 ± 3.8010i	3.41	0.61
p_2	-0.1908 ± 4.0096i	4.75	0.64
p_3	-0.0308 ± 3.4620i	0.89	0.55
UOP	0.0178 ± 2.5614i	-0.69	0.41

of SGs, line currents, and power flows, it is determined that rotor angles (δ_1 and δ_2) of G_1 and G_2 exhibit higher values of GMO and therefore are selected to design RWDC in the proposed work.

C. CONTROLLER IMPLEMENTATION

To construct a controller for the uncertain polytopic system of the WPTBS, model linearizing is performed at each operating point listed in TABLE 1. The SMA method [10], [23] is applied to reduce the size of each LTI model to include only the relevant modes i.e., two local modes and one IAM for the employed test system. By selecting G_3 as the reference machine, the 6^{th}-order model, having complex eigenvalues equivalent to the full-order system, is obtained. The second-order time delay model is then combined with each reduced-order system, eventually producing $\hat{A}_j$, $\hat{B}_j$, and $\hat{C}_j$ LTI matrices of size 10×10, 10×1, and 2×10, respectively, for each operating point. A fixed time-delay value of $T_d = 150$ms is considered for all the vertices. Finally, by forming a set of three $\hat{C}_j^i$ matrices (12) for each operating point to accommodate the permanent communication failure according to (13), a polytopic system comprising nine vertices ($\mathcal{P}_1$, $\mathcal{P}_2 \ldots \mathcal{P}_9$) is obtained.

The parameter-dependent LMI conditions are solved in MATLAB using a computational package comprising a Robust LMI parser [33] and Mosek solver [34]. The feasible solution with an adequate damping ratio (i.e., at least 10% for each vertex) is obtained by setting $\mu = 8$, $g = \{1\ 1\ 0\}$, and $n_c = 2$. The resulting parameters of the controller are stated in (26) or (27).

$$K_c = \begin{bmatrix} -5.94 & -8.63 & 1.85 & -6.10 \\ 1.91 & 1.88 & 0.69 & 2.40 \\ -0.99 & 1.97 & -4.00 & -5.19 \end{bmatrix} \quad (26)$$

$$A_c = \begin{bmatrix} -5.94 & -8.63 \\ 1.91 & 1.88 \end{bmatrix},\ B_c = \begin{bmatrix} 1.85 & -6.10 \\ 0.69 & 2.40 \end{bmatrix},$$
$$C_c = \begin{bmatrix} -0.99 & 1.97 \end{bmatrix},\ D_c = \begin{bmatrix} -4.00 & -5.19 \end{bmatrix} \quad (27)$$

It is to be noted that the computational complexity of the proposed approach mainly depends on the number of operating points and vertices considered at the design stage, the order of each vertex (LTI model), and the degree of polynomial for the Lyapunov matrices. The implementations for the controller synthesis are carried out using MATLAB 9.8.0 (2020a) on a Desktop PC with an Intel (R) Corei5 2.80 GHz processor and 16 GB of RAM. It took 25.8 s of computing time to determine the controller parameters (26) using the proposed LMI approach.

D. CLOSED-LOOP EIGENVALUE ANALYSIS

The closed-loop eigenvalues are then shown in Fig 5-Fig 7 for different cases to analyze the damping level of the IAM under operating point uncertainty, time delays, and communication loss. As indicated in Fig 5, the ζ of the IAM remains well above 25% for all operating points, even for the UOP which was not considered at the design stage. The complex plot, depicted in Fig 6 illustrates that the closed-loop performance deteriorates with a total time delay of 300 ms in both communication channels, particularly for the p_3 and UOP, but it still exceeds 10%, which is acceptable with such large time delays. Moreover, from the eigenvalue plot shown in Fig 7 (a)-(b), it is inferred that the ζ of the IAM remains over 15% for all operating points in case one of the wide-area channels fails. Next, the eigenvalue results will be verified by conducting non-linear time-domain simulations.

V. SIMULATION RESULTS

The time-domain simulations are carried out to evaluate the effectiveness of the proposed approach under different scenarios, as listed in TABLE 2. These scenarios assess the performance of the controller against uncertainty in operating points, time delays, and communication failure subject to different disturbances. Besides, to highlight the superiority of the proposed approach over existing methods, comparative simulation results are also presented by designing WADCs based on the phase compensation method [11],

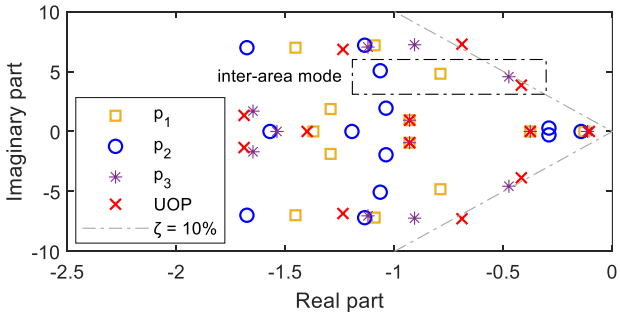

FIGURE 6. Eigenvalue plots for different operating points and 300 ms time delay.

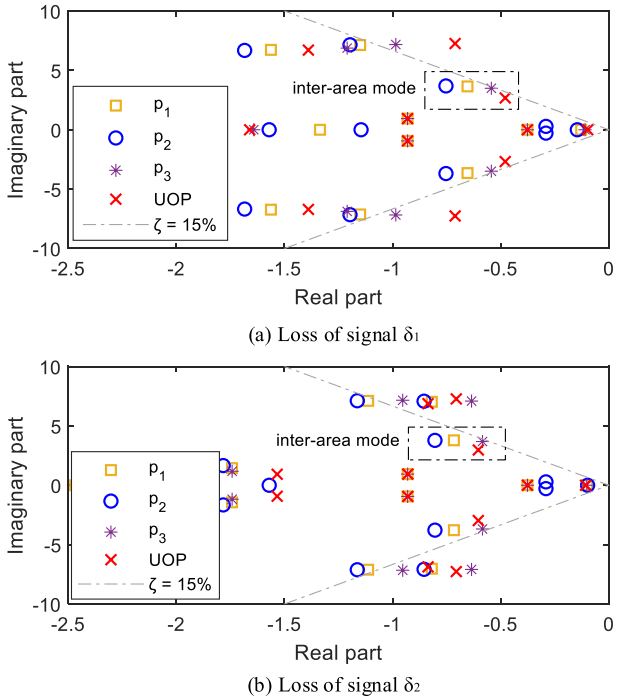

(a) Loss of signal δ_1

(b) Loss of signal δ_2

FIGURE 7. Eigenvalue plot for different operating points and communication failures.

mixed-sensitivity H_∞ control [12], and polytopic-based H_2 WADC [1].

A. SCENARIO A

In this scenario, at $t = 1$ s, the WPTBS undergoes a three-phase fault at bus 8 for 80 ms duration. The obtained simulation results are depicted in Fig 8 and Fig 9, respectively, for the operating points p_3 and UOP. The comparative results evidently demonstrate the dominant performance of the proposed approach for mitigating LFOs with the smallest settling time and lesser fluctuations. For transient simulations, the maximum power output from the DFIG is set to 180 MW to avoid the over-current in the rotor winding. Assuming $Q_{s_{ref}} = 0$ during steady-state, the reactive power deviations ΔQ_{max} to ΔQ_{min} from the RSC is fixed at -1.1 pu to $+0.75$ pu, respectively, as shown in Fig 8 (d).

TABLE 2. Case Scenarios for evaluating the performance of the controller.

Scenario	Operating points	Time delays	Loss of signal	Dynamic disturbance
A	p_3 UOP			Three-phase fault
B	p_1	100 ms in δ_1 200 ms in δ_2		Excitation voltage change
	p_3	Variable delay in δ_1		
	UOP	150 ms in δ_2		
C	p_1		δ_2	Load variations
	p_3		δ_1	
Worst case	UOP	125 ms in δ_2	δ_1	Line tripping

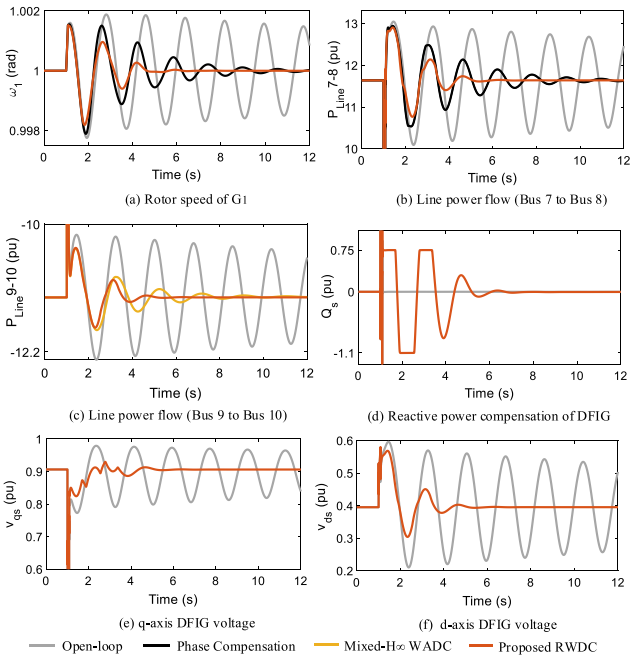

FIGURE 8. Scenario A: Dynamic responses for p_3.

B. SCENARIO B

The reference excitation voltages of all SGs are increased by 0.05 pu for 200 ms to generate the dynamic disturbance in this case. The transient results, shown in Fig 10 (a)-(b) for p_1 with associated delays (stated in TABLE 2), demonstrate that better performance can be obtained if time delays are incorporated at the design stage. Furthermore, the comparative results shown in Fig 11, also validate the effectiveness of the proposed approach under variable delays. Besides, from Fig 12, it can be inferred that the performance of the mixed-H_∞ control method might be comparable to that of the proposed approach. However, the controller designed using the former approach is of the 6^{th} order and can only be designed for one operating point.

C. SCENARIO C

In this scenario, the performance of the controller is evaluated under the loss of wide-area feedback signals, as stated in TABLE 2. A dynamic disturbance at bus 9 causes the

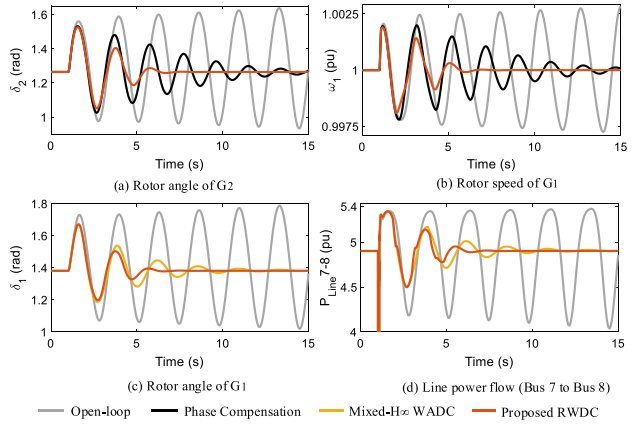

FIGURE 9. Scenario A: Dynamic responses for UOP

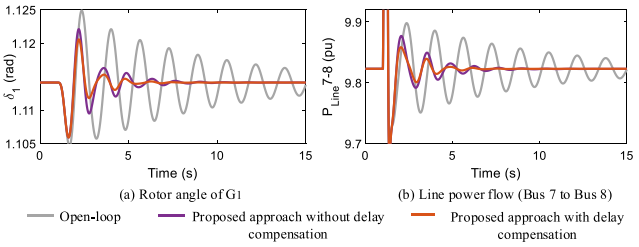

FIGURE 10. Scenario B: Dynamic responses for p_1 with different fixed delays in both communication channels.

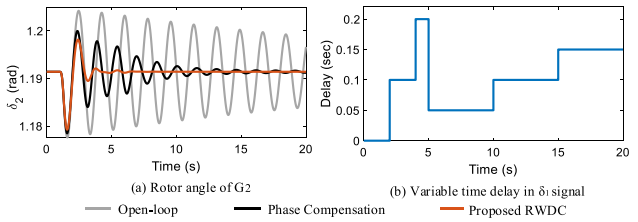

FIGURE 11. Scenario B: Dynamic responses for p_3 with variable delay.

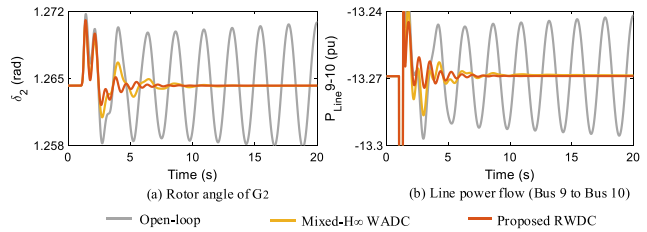

FIGURE 12. Scenario B: Dynamic responses for UOP with a fixed-delay in δ_2 signal.

successive tripping of a 100 MW load at time intervals of 1 and 10 seconds. The comparative transient results illustrated in Fig 13 and Fig 14 for different operating points and wide-area signal failure indicate that the proposed approach delivers robust performance for suppressing LFOs if one of the feedback signals is lost, relative to a polytopic-based

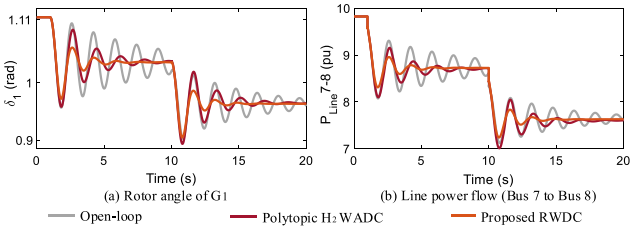

FIGURE 13. Scenario C: Dynamic responses for p_1 with the loss of δ_2 signal.

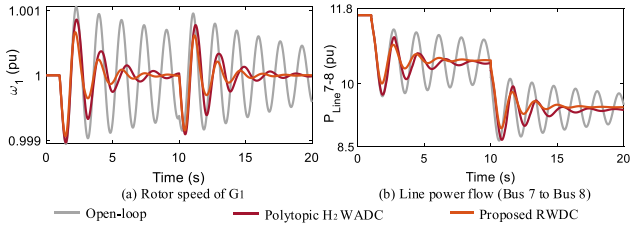

FIGURE 14. Scenario C: Dynamic responses for p_3 with the loss of δ_2 signal.

WADC [1]. Moreover, this approach solved the LMI optimization problem in 75.5 s and yielded a 5th-order controller. This ensures better computational efficiency and less complexity for the proposed approach.

D. WORST CASE SCENARIO

Given the worst-case scenario stated in TABLE 2, the WPTBS undergoes a line-tripping fault at one of the tie-lines connecting bus 7 and bus 8 for 50 ms. Moreover, the fluctuations in the wind speed and solar irradiance are depicted in Fig 15 (a)-(b). From dynamic responses shown in Fig 15 (c)-(f), it can be concluded that even under a critical scenario, the controller provides adequate damping by rapidly mitigating the oscillations.

VI. CONCLUSION

This work presented a reduced-order RWDC for the WPTBS to suppress LFOs while accounting for multiple operating points, time delays, and permanent communication failures. A robust dynamic OFC was designed by minimizing the H_∞ norm using a two-stage LMI framework. Firstly, the polytopic model was constructed using three distinct operating points, considering uncertainties in the output power of wind-PV-thermal resources, different load demands, and varying tie-line power flows, followed by incorporating fixed time delays and communication failures associated with wide-area signals. Afterward, an LMI algorithm, which ensured required damping level for the entire uncertainty model by selecting a pre-defined order of the controller and PDLFs of assigned degrees, was proposed to accomplish the design of RWDC.

Finally, from the small-signal analysis and simulation results for various scenarios, it is concluded that the resulting

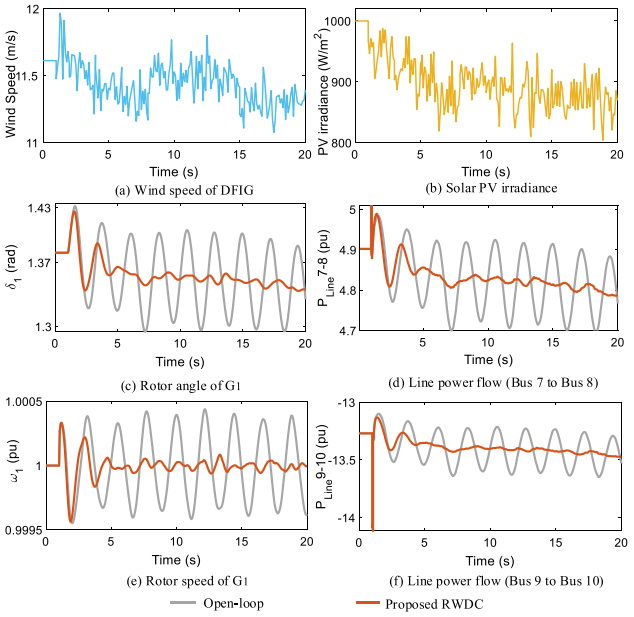

FIGURE 15. Dynamic responses for worst-case scenario.

second-order controller not only provided higher robustness for the given set of operating points compared to existing methods but also guaranteed a sufficient damping ratio for the unstable dominant mode case, over fixed or variable time delays, and in the event of communication loss.

From the real application viewpoint, the implementation of the suggested approach becomes complicated on practical large-scale power grids containing thousands of buses. The major challenge lies in increased complexity, essentially owing to the need to model the power system components for such complex systems. The proposed approach can address this challenge by employing advanced equivalence methods to reduce the power network size or exploring alternative model reduction methods, enabling the feasibility of the proposed approach for those practical power systems, which will be our main focus in future research. This will allow us to provide valuable insights on its potential applications for improving the stability of larger power networks.

REFERENCES

[1] R. Sadiq, Z. Wang, and C. Y. Chung, "A multi-model multi-objective robust damping control of GCSC for hybrid power system with offshore/onshore wind farm," *Int. J. Electr. Power Energy Syst.*, vol. 147, May 2023, Art. no. 108879.

[2] P. He, Q. Fang, H. Jin, Y. Ji, Z. Gong, and J. Dong, "Coordinated design of PSS and STATCOM-POD based on the GA-PSO algorithm to improve the stability of wind-PV-thermal-bundled power system," *Int. J. Electr. Power Energy Syst.*, vol. 141, Oct. 2022, Art. no. 108208.

[3] C. Yan, W. Yao, and J. Wen, "Impact of active frequency support control of photovoltaic on PLL-based photovoltaic of wind-photovoltaic-thermal coupling system," *IEEE Trans. Power Syst.*, vol. 38, no. 5, pp. 4788–4799, Sep. 2022.

[4] M. Basu, J. Kim, R. M. Nelms, and E. Muljadi, "Coordination of utility-scale PV plant and wind power plant in interarea-oscillation damping," *IEEE Trans. Ind. Appl.*, vol. 59, no. 4, pp. 4744–4751, Jul. 2023.

[5] A. Faraji, A. H. Naghshbandy, and A. G. Baayeh, "A hybrid coordinated design method for power system stabilizer and FACTS device based on synchrosqueezed wavelet transform and stochastic subspace identification," *J. Modern Power Syst. Clean Energy*, vol. 9, no. 4, pp. 910–918, Jul. 2021.

[6] Y. Hu, S. Bu, X. Zhang, C. Y. Chung, and H. Cai, "Connection between damping torque analysis and energy flow analysis in damping performance evaluation for electromechanical oscillations in power systems," *J. Modern Power Syst. Clean Energy*, vol. 10, no. 1, pp. 19–28, Jan. 2022.

[7] A. Kumar and M. Bhadu, "Wide-area damping control system for large wind generation with multiple operational uncertainty," *Electr. Power Syst. Res.*, vol. 213, Dec. 2022, Art. no. 108755.

[8] M. E. C. Bento, "A hybrid particle swarm optimization algorithm for the wide-area damping control design," *IEEE Trans. Ind. Informat.*, vol. 18, no. 1, pp. 592–599, Jan. 2022.

[9] M. E. C. Bento and R. A. Ramos, "A method based on linear matrix inequalities to design a wide-area damping controller resilient to permanent communication failures," *IEEE Syst. J.*, vol. 15, no. 3, pp. 3832–3840, Sep. 2021.

[10] P. Gupta, A. Pal, and V. Vittal, "Coordinated wide-area damping control using deep neural networks and reinforcement learning," *IEEE Trans. Power Syst.*, vol. 37, no. 1, pp. 365–376, Jan. 2022.

[11] W. Yao, L. Jiang, J. Wen, Q. H. Wu, and S. Cheng, "Wide-area damping controller of FACTS devices for inter-area oscillations considering communication time delays," *IEEE Trans. Power Syst.*, vol. 29, no. 1, pp. 318–329, Jan. 2014.

[12] S. Zhang and V. Vittal, "Wide-area control resiliency using redundant communication paths," *IEEE Trans. Power Syst.*, vol. 29, no. 5, pp. 2189–2199, Sep. 2014.

[13] Y. Shen, W. Yao, J. Wen, H. He, and L. Jiang, "Resilient wide-area damping control using GrHDP to tolerate communication failures," *IEEE Trans. Smart Grid*, vol. 10, no. 3, pp. 2547–2557, May 2019.

[14] A. Movahedi, A. H. Niasar, and G. B. Gharehpetian, "Designing SSSC, TCSC, and STATCOM controllers using AVURPSO, GSA, and GA for transient stability improvement of a multi-machine power system with PV and wind farms," *Int. J. Electr. Power Energy Syst.*, vol. 106, pp. 455–466, Mar. 2019.

[15] M. J. Morshed and A. Fekih, "A probabilistic robust coordinated approach to stabilize power oscillations in DFIG-based power systems," *IEEE Trans. Ind. Informat.*, vol. 15, no. 10, pp. 5599–5612, Oct. 2019.

[16] M. Darabian and A. Bagheri, "Stability improvement of large-scale power systems including offshore wind farms and MTDC grid aiming at compensation of time delay in sending robust damping signals," *Int. J. Electr. Power Energy Syst.*, vol. 143, Dec. 2022, Art. no. 108491.

[17] A. Prakash, R. K. Tiwari, K. Kumar, and S. K. Parida, "Interacting multiple model strategy based adaptive wide-area damping controller design for wind farm embedded power system," *IEEE Trans. Sustain. Energy*, vol. 14, no. 2, pp. 962–973, Apr. 2023.

[18] Z. Zhang and X. Zhao, "Coordinated power oscillation damping from a VSC-HVDC grid integrated with offshore wind farms: Using capacitors energy," *IEEE Trans. Sustain. Energy*, vol. 14, no. 2, pp. 751–762, Apr. 2023.

[19] Y. Zhou, L. Qin, and Y. Li, "Output-feedback photovoltaic WADC by H_∞ criterion using auxiliary function," *Int. J. Electr. Power Energy Syst.*, vol. 136, Mar. 2022, Art. no. 107603.

[20] R. K. Varma and M. Akbari, "Simultaneous fast frequency control and power oscillation damping by utilizing PV solar system as PV-STATCOM," *IEEE Trans. Sustain. Energy*, vol. 11, no. 1, pp. 415–425, Jan. 2020.

[21] H. Silva-Saravia, H. Pulgar-Painemal, L. M. Tolbert, D. A. Schoenwald, and W. Ju, "Enabling utility-scale solar PV plants for electromechanical oscillation damping," *IEEE Trans. Sustain. Energy*, vol. 12, no. 1, pp. 138–147, Jan. 2021.

[22] H. Setiadi, N. Mithulananthan, and R. Shah, "Design of wide-area POD with resiliency using modified DEA for power systems with high penetration of renewable energy," *IET Renew. Power Gener.*, vol. 13, no. 2, pp. 342–351, Feb. 2019.

[23] Y. Zhou, J. Liu, Y. Li, C. Gan, H. Li, and Y. Liu, "A gain scheduling wide-area damping controller for the efficient integration of photovoltaic plant," *IEEE Trans. Power Syst.*, vol. 34, no. 3, pp. 1703–1715, May 2019.

[24] Y. Pipelzadeh, N. R. Chaudhuri, B. Chaudhuri, and T. C. Green, "Coordinated control of offshore wind farm and onshore HVDC converter for effective power oscillation damping," *IEEE Trans. Power Syst.*, vol. 32, no. 3, pp. 1860–1872, May 2017.
[25] C. M. Agulhari, R. C. L. F. Oliveira, and P. L. D. Peres, "LMI relaxations for reduced-order robust H_∞ control of continuous-time uncertain linear systems," *IEEE Trans. Autom. Control*, vol. 57, no. 6, pp. 1532–1537, Jun. 2012.
[26] B. Pal and C. Balarko, *Robust Control in Power Systems*. New York, NY, USA: Springer, 2005.
[27] M. Francoise, "Small-signal modelling and analysis of doubly-fed induction generators in wind power," Ph.D. dissertation, Imperial College London, Univ. London, London, U.K., 2007.
[28] Q. Wang, W. Yao, J. Fang, X. Ai, J. Wen, X. Yang, H. Xie, and X. Huang, "Dynamic modeling and small signal stability analysis of distributed photovoltaic grid-connected system with large scale of panel level DC optimizers," *Appl. Energy*, vol. 259, Feb. 2020, Art. no. 114132.
[29] F. R. Segundo Sevilla, I. Jaimoukha, B. Chaudhuri, and P. Korba, "Fault-tolerant control design to enhance damping of inter-area oscillations in power grids," *Int. J. Robust Nonlinear Control*, vol. 24, nos. 8–9, pp. 1304–1316, May 2014.
[30] A. M. Souza, R. C. L. F. Oliveira, and P. L. D. Peres, "H_∞ model match output-feedback control by means of an LMI-based algorithm," *IEEE Control Syst. Lett.*, vol. 6, pp. 560–565, 2022.
[31] R. Sadiq, Z. Wang, and C. Y. Chung, "Coordinated robust PID-based damping control of permanent magnet synchronous generators for low-frequency oscillations considering power system operational uncertainties," *J. Mod. Power Syst. Clean Energy*, early access, Sep. 1, 2023.
[32] P. Kundur, *Power System Stability and Control*. New York, NY, USA: McGraw-Hill, 1994.
[33] C. M. Agulhari, A. Felipe, R. C. L. F. Oliveira, and P. L. D. Peres, "Algorithm 998: The robust LMI parser—A toolbox to construct LMI conditions for uncertain systems," *ACM Trans. Math. Softw.*, vol. 45, no. 3, pp. 1–25, Sep. 2019.
[34] E. D. Andersen and K. D. Andersen, *The Mosek Interior Point Optimizer for Linear Programming: An Implementation of the Homogeneous Algorithm*. Boston, MA, USA: Springer, 2000.

ZHEN WANG (Member, IEEE) received the B.Eng. degree from Xi'an Jiaotong University, Xi'an, China, in 1998, the M.Eng. degree from Zhejiang University, Hangzhou, China, in 2001, and the Ph.D. degree from The Hong Kong Polytechnic University, Hong Kong, China, in 2009. He is currently a full-time Professor and the Director of the Institute of Power and Energy Integration and Intelligence, Zhejiang University. His research interests include power system stability and control, renewable energy integration, and voltage source converter-based high-voltage direct current (VSC-HVDC) transmission. He is an Expert Member of the IEC TC8/SC8B/JWG1 Working Group on Microgrid Operation and Control and a member of some topical advisory panels. He was a recipient of the 2014 Endeavour Research Fellowship sponsored by Australian Government and a Visiting Scholar of The University of Western Australia, Perth, Australia. He serves as an Editor for *Electronics*.

REHAN SADIQ received the B.Eng. and M.Eng. degrees from the University of Engineering and Technology, Taxila, Pakistan, in 2012 and 2015, respectively. He is currently pursuing the Ph.D. degree with the College of Electrical Engineering, Zhejiang University, Hangzhou, China. His research interests include power system stability and control with renewable energy penetration and flexible AC transmission systems (FACTS).

DEQIANG GAN (Senior Member, IEEE) received the Ph.D. degree in electrical engineering from Xi'an Jiaotong University, Xi'an, China, in 1994. He held research positions with Ibaraki University, Ibaraki, Japan, the University of Central Florida, Orlando, FL, USA, and Cornell University, Ithaca, NY, USA, from 1994 to 1998. He was with ISO New England Inc., Holyoke, MA, USA, from 1998 to 2002. He has been a Faculty Member with Zhejiang University, Hangzhou, China, since 2002. He visited The University of Hong Kong, Hong Kong, China, in 2004, 2005, and 2006. He served as an Editor for *European Transactions on Electrical Power*, from 2007 to 2014. His research interests include power system stability and control.